Relativistic Nondipole Effects in Strong-Field Atomic Ionization at Moderate Intensities

Nida Haram,[1,*] Igor Ivanov,[2,†] Han Xu,[1,‡] Kyung Taec Kim,[2,3] A. Atia-tul-Noor,[1] U. Satya Sainadh,[1,¶] R. D. Glover,[1] D. Chetty,[1] I. V. Litvinyuk,[1,§] and R. T. Sang[1,‖]

[1]*Centre for Quantum Dynamics, Griffith University, Brisbane, Queensland 4111, Australia*

[2]*Centre for Relativistic Laser Science, Institute for Basic Science, Gwangju, 61005, Republic of Korea*

[3]*Department of Physics and Photon Science, Gwangju Institute of Science and Technology, Gwangju 61005, Korea*

(Received 2 August 2018; published 28 August 2019)

We present a detailed experimental and theoretical study on the relativistic nondipole effects in strong-field atomic ionization by near-infrared linearly polarized few-cycle laser pulses in the intensity range of 10^{14}–10^{15} W/cm^2. We record high-resolution photoelectron momentum distributions of argon using a reaction microscope and compare our measurements with a truly *ab initio* fully relativistic 3D model based on the time-dependent Dirac equation. We observe counterintuitive peak shifts of the transverse electron momentum distribution in the direction opposite to that of laser propagation as a function of laser intensity and demonstrate an excellent agreement between the experimental results and theoretical predictions.

DOI: 10.1103/PhysRevLett.123.093201

In strong-field atomic or molecular ionization with near- and midinfrared lasers, relativistic effects are known to appear at laser intensities over 10^{18} W/cm^2 [1] because, depending on the laser wavelength, the photoelectrons can gain sufficiently high ponderomotive energy that their velocity can approach speed of light in the vacuum. However, the onset of relativistic nondipole effects becomes noticeable even at moderately intense (10^{13}–10^{14} W/cm^2) low frequency (mid- and near-infrared) laser fields. These nondipole effects appear as a result of the high energy electrons in the laser field being affected by the magnetic field component of the light pulse, which induces a non-negligible momentum transfer to the photoelectrons [2,3]. To understand and describe these effects, theoretical modelling must extend beyond the dipole approximation, which neglects the small photon momentum by assuming the magnetic field component of the laser field to be zero, resulting in no momentum being transferred to the photoelectrons along the laser propagation direction. In addition, these effects cannot be fully explained without taking into account the Coulomb interaction between the photoelectron and the parent ion, hence going beyond the strong-field approximation (SFA). In the case of a linearly polarized laser field, the Coulomb attraction imparts the momentum in the transverse direction and draws the photoelectron towards the parent ion, leading to the focusing effect [4,5]. Therefore, the combined effect of the Lorentz force and Coulomb attraction from the parent ion contributes to these nondipole effects. Such nondipole effects may have a direct implication on many important phenomena relying on the recollision process, such as holography with photoelectrons [6,7], high harmonic generation [8], laser induced electron diffraction [9–11], and frustrated tunneling ionization [12].

Relativistic nondipole effects are revealed in the ionized photoelectron momentum spectra, which are acquired as a result of strong-field atomic ionization. It was reported experimentally that, for a circularly polarized laser field (800 and 1400 nm, $\sim 10^{14}$ W/cm^2), the ionized photoelectrons gain forward momentum in the laser propagation direction due to the radiation pressure effect [2]. The momentum gain is manifested as an asymmetry in the electron momentum distribution (EMD), which can be quantified by extracting a translational shift of the electron momentum spectrum through the measurement of the peak momentum shift. This overall momentum gain from the field is related to the expectation value of electron momentum in the pulse propagation direction. This value is positive and is well reproduced by the classical [2,13] and semiclassical [14] theoretical models. Successful attempts were made using theoretical models in the relativistic framework that employs a relativistic strong-field approximation [15,16] and a time-dependent Dirac equation [17]. In another experiment performed with a linearly polarized low-frequency laser field (3400 nm, $\sim 10^{13}$ W/cm^2) [3], negative peak shifts were reported. A more complex picture emerged when the photoelectron momentum distribution was analyzed in detail. The transverse photoelectron momentum is shifted forward along the pulse propagation direction only on average. The so-called direct electrons, which never recollide with the parent ion, are driven in the direction of the laser photon momentum. However, a fraction of slow electrons, which can experience recollision, acquire momentum opposite to the photon momentum. This complex behavior was shown to be the result of interplay between the Lorentz force and Coulomb attraction [18]. Several theoretical models were developed to describe these counterintuitive peak shifts, which include

semiclassical models [3,19] and SFA theories, such as a nondipole SFA theory based on exact nondipole Volkov solutions for the time-dependent Schrödinger equation (TDSE) [20] and a nondipole quantum trajectory-based Coulomb-corrected SFA theory [21]. However, proper treatment of such effects clearly necessitates a correct description of both relativistic and Coulomb effects. In [18], such a description was based on the solution of the TDSE for a model 2D hydrogen atom described by a soft-core potential. In [22], these effects were accounted for using the perturbative treatment of the relativistic nondipole interactions.

In the present work, we use a theoretical model based on the numerical solution of the 3D time-dependent Dirac equation (3D-TDDE). An approach based on the 3D-TDDE allows a truly *ab initio* description of the relativistic effects, and it has been advocated recently by different groups [17,23]. Such relativistic development of the theory is indispensable for the description of the ionization phenomena occurring for the currently available field intensities on the order of 10^{18} W/cm^2 and higher. The approach based on the Dirac equation incorporates relativistic effects, such as the nondipole effects, effects of the relativistic kinematics, and spin-orbit interactions in the most natural way. Compared to the more traditional approaches, such as treating the relativistic effects in the framework of the lowest order perturbation theory, the approach based on the 3D-TDDE also offers an advantage of a technical character, which may be quite useful in practical calculations. Indeed, some terms of the Breit-Pauli Hamiltonian [24] describing relativistic interactions in the lowest order perturbation theory are highly singular operators. The spin-orbit interaction operator and the Darwin term, for instance, exhibit the $1/r^3$ and delta-function singularities at the origin, respectively. Treatment of such singular behavior in a numerical calculation necessitates the use of various *ad hoc* regularization techniques. Solution of the 3D-TDDE, on the other hand, does not pose such technical problems. The price to pay for this advantage is a somewhat higher computational cost that is not, however, an insurmountable obstacle. In the regime of the moderately intense fields considered in this work, we obtain accurate experimental results for the relativistic effects, thereby providing an opportunity for a precise comparison between theory and experiment.

In our experiment, as shown in Fig. 1, a linearly polarized few-cycle pulse (~6 fs and ~740 nm, produced by a *Femtopower Compact Pro CE Phase* amplified laser system) propagating along the y axis is focused on a supersonic Ar jet, which is propagating along the x axis. The peak intensity of the few-cycle pulse is varied by a set of pellicle beam splitters to cover a range of $6 \times 10^{14} - 3 \times 10^{15}$ W/cm^2. A Berek compensator is used to achieve linear polarization of the light pulses, where the inherent ellipticity in the few-cycle pulses is removed by a

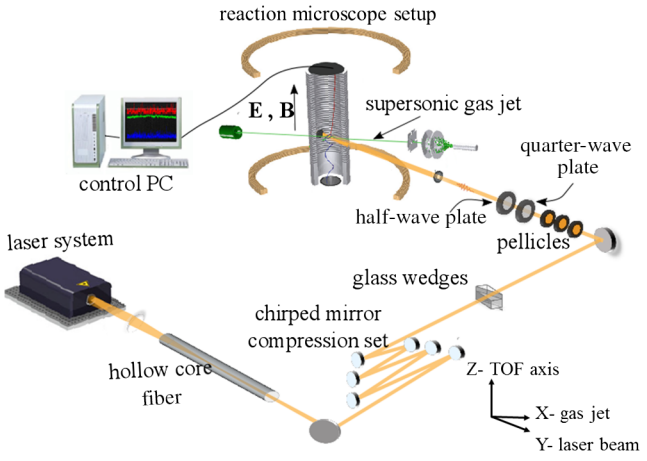

FIG. 1. Schematic of the experimental setup.

quarter-wave plate. A half-wave plate then rotates the polarization axis to the z axis [time-of-flight (TOF) axis of a reaction microscope (REMI)]. A pair of fused silica wedges with adjustable insertion can compensate for the chirp of the few-cycle pulses, minimizing the pulse duration in the interaction region. The *in situ* laser intensity in the interaction region is precisely calibrated by the recoil-ion momentum imaging method [25,26] within 10% confidence. The space charge effect is avoided by carefully controlling the Ar jet density for different laser intensities to achieve a low ionization rate of < 1 ionization event per pulse.

Full 3D photoelectron momentum distributions from the strong-field ionization of Ar atoms are recorded by a REMI [27]. In order to ensure that the considered electrons are from Ar^+, both the ions and electrons are measured in coincidence with only those electron-ion pairs that mutually conserved momentum.

Owing to the importance of the Coulomb interaction between the parent ion and the ejected photoelectron in the linearly polarized laser field [28–33], the transverse electron momentum distribution (TEMD)—perpendicular to the polarization plane of the laser field—is used to gain insight into the details of the recollision event without it being obscured by the large momentum transfer from the laser field. The information about the relativistic nondipole effects is hidden in the fine details of the TEMD along the laser propagation direction. The TEMD is recorded by a REMI with sufficiently high resolution to resolve the nondipole effect induced momentum peak shift in the laser propagation direction. The typical 2D photoelectron momentum distributions are presented in Fig. 2(a). The 2D photoelectron momentum spectrum integrated over the y axis evolves into a cusp, as shown in Fig. 2(b). The cusp profile of the TEMD—centered at zero transverse momentum P_y—is attributed to the Coulomb focusing effect [4,5,28,34], which implies that the ionized photoelectron is attracted towards the parent ion due to the momentum

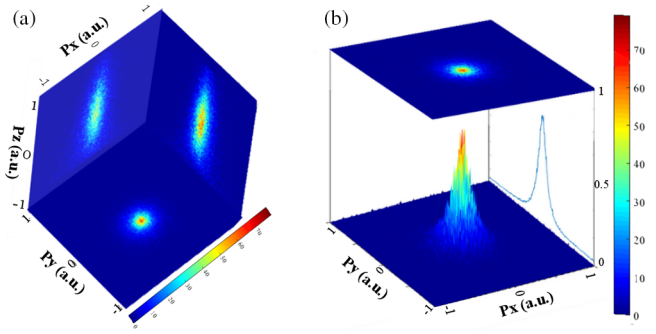

FIG. 2. (a) Measured electron momentum distributions projected onto three orthogonal planes recorded at $6 \times 10^{14}\,\mathrm{W/cm^2}$. (b) Evolution of cusp in the TEMD obtained with an intensity of 6×10^{14} $\mathrm{W/cm^2}$.

transfer in the transverse direction as a consequence of the Coulomb attraction.

To scale the features of the cusp for a better discernment, the plot of the ionization rate $W(P_y)$ is used. The function $V(P_y) = \ln W(P_y)$ is then analyzed in a narrow range of transverse photoelectron momenta $|P_y| \leq 0.5$ a.u. (a.u. refers to atomic units) [5]. We observed that the cusp profile of the TEMD exhibits slight asymmetry, which becomes more pronounced as the intensity increases. The asymmetry is extracted in the form of the peak shift, which is the key observable in this experiment to explore the relativistic nondipole effects. For the TEMD to have a cusp profile, $V(P_y)$ should have a singularity at its maximum near the point $P_y = 0$, which can be described by representing $V(P_y)$ in the vicinity of the maximum as [5,35]

$$V(P_y) = B + A|P_y - \beta|^{\alpha}. \tag{1}$$

The experimental data are fitted with the same function $V(P_y)$ by performing a series of least square fits, as shown in Fig. 3. The coefficients A, B, α, and β are the fitting parameters. A and B are expansion coefficients, α describes the shape of the TEMD ($\alpha \to 1.35$ for the present case), and β accounts for the peak shift $\langle P_y \rangle$. The peak shifts $\langle P_y \rangle$ as a function of laser intensity are extracted with reference to the data obtained at the lowest intensity.

To obtain theoretical predictions, we solve the time-dependent Dirac equation (TDDE)

$$i\frac{\partial \Psi(r,t)}{\partial t} = \hat{H}\Psi(r,t) \tag{2}$$

for the bispinor $\Psi(r,t)$ with the Hamiltonian operator

$$\hat{H} = \hat{H}_{\mathrm{atom}} + \hat{H}_{\mathrm{int}}, \tag{3}$$

with

$$\hat{H}_{\mathrm{atom}} = c\boldsymbol{\alpha}\cdot\hat{\boldsymbol{p}} + c^2(\beta - I) + IV(r) \tag{4}$$

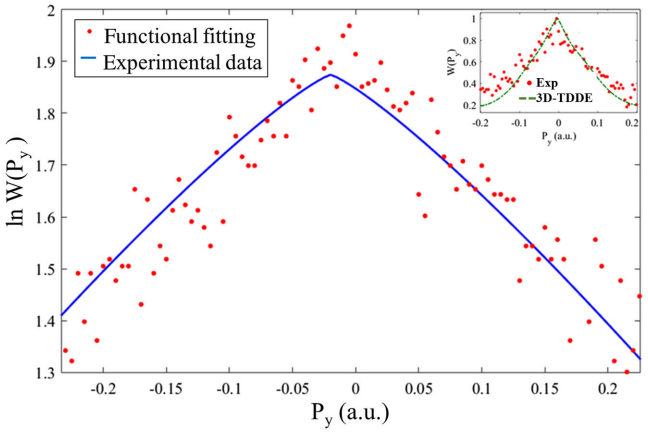

FIG. 3. Projection of TEMD onto the laser beam propagation axis at intensity of 6.5×10^{14} $\mathrm{W/cm^2}$ fitted with the function $V(P_y)$. Inset figure shows the normalized ionization rate obtained from theoretical and experimental data.

and

$$\hat{H}_{\mathrm{int}} = c\boldsymbol{\alpha}\cdot\hat{\boldsymbol{A}}, \tag{5}$$

Here, $\boldsymbol{\alpha}$ and β are Dirac matrices, and $c = 137.036$ is the speed of light in atomic units.

The pulse is defined in terms of vector potential $\boldsymbol{A}(\boldsymbol{y},t)$ that, when nondipole effects are included in consideration, is a function of temporal and spatial variables $A(t - y/c)$ for the pulse propagating in the y direction and is given as

$$\hat{\boldsymbol{A}}(\boldsymbol{y},t) = -\frac{\hat{\boldsymbol{E}}}{\omega}\sin^2\left(\frac{\pi u}{T_1}\right)\cos(\omega u + \phi) \tag{6}$$

for $0 < u < T_1$, and it is zero elsewhere.

Here, $u = t - y/c$; $\boldsymbol{E}$ is the field strength; the carrier frequency ω is 0.059205 a.u. corresponding to a wavelength of 770 nm; $T_1 = 5 \times 2\pi/\omega$ corresponds to the pulse duration of 6 fs; and ϕ is the carrier envelope phase (CEP), which is zero in all the calculations.

We use the single-active-electron approximation (SAE) to describe the target atom, employing a model potential $V(r)$ [36] in Eq. (4). The solution is sought as a series in basis bispinors:

$$\Psi(\mathbf{r},t) = \sum_{\substack{j \\ l=j\pm 1/2}} \sum_{M=-j}^{j} \Psi_{jlM}(\boldsymbol{r},t). \tag{7}$$

A detailed description of the procedure used to solve the TDDE numerically can be found in [17]. The photoelectron momentum distribution is obtained by projecting the solution of the TDDE after the end of the pulse on the set of the scattering states of the Dirac Hamiltonian [Eq. (4)] with ingoing boundary conditions.

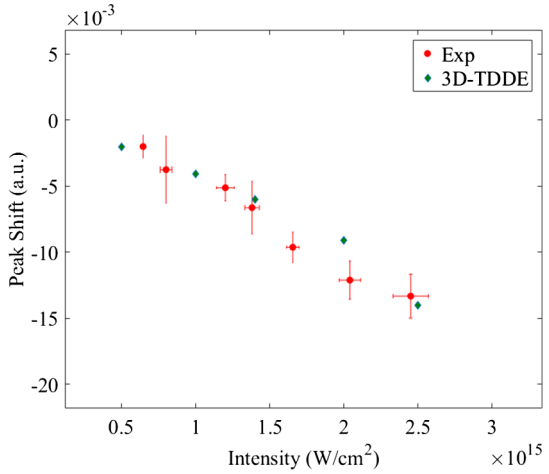

FIG. 4. The relative peak shift $\langle P_y \rangle$ extracted from experiment and theory agree well in the entire intensity range.

In Fig. 4, the experimental results are compared with theoretical predictions with error bars on both the intensity and peak shift. The horizontal error bars depict uncertainty in the intensity due to systematic errors, whereas the confidence bounds of the fitting parameter β serve as error bars on the peak shifts. Clearly, we observe increasing counterintuitive peak shifts with increasing laser intensities due to the effect of the attractive Coulomb force on the low energy electrons. The experimental and theoretical results are in quite good agreement within the entire intensity range.

In order to unravel the effect of long-range Coulomb potential on the peak shift, we performed simulations for a model Ar atom with Yukawa-type potential, which is a short-range screened Coulomb potential,

$$V(r) = -g^2 \frac{e^{-\alpha r}}{r}, \tag{8}$$

with g^2 and α as the scaling constants, and m as the mass of electron. The simulations were performed for two different values of the Yukawa potential, with scaling constants $[g^2 = 2.61, \alpha = 0.1]$ and $[g^2 = 3.38, \alpha = 0.3]$, respectively. The particular values for the scaling constants were chosen such that the system has the ionization energy close to that of the Ar atom in the initial p state. We used the initial p state for the ionization in the Yukawa potential so that all the relevant details of the initial state (energy and angular momentum) would mimic those of the Ar atom closely, as well as to demonstrate the effect of the Coulomb potential unambiguously. The simulations were performed with the same pulse parameters as used in the previous simulations at an intensity of 2.5×10^{15} W/cm^2, where the effect of the Coulomb potential was most pronounced. The comparison of the peak shifts extracted from the simulations performed for the Coulomb potential and the Yukawa potentials is depicted in Fig. 5. All the curves are normalized to unity in order to highlight the relative peak shift. We observe that the long-range Coulomb potential shows the greatest peak shift, whereas the shortest range $[g^2 = 3.38, \alpha = 0.3]$ of the Yukawa potential results in the least peak shift—attributed to the fact that it is unable to attract the electron towards the parent ion significantly. The intermediate value of the Yukawa potential $[g^2 = 2.61, \alpha = 0.1]$, as expected, yields a peak shift lying between the two extreme cases, which is sufficient to conclude that counterintuitive peak shifts of TEMD definitely result from the longer range Coulomb attraction of the parent ion.

To demonstrate the requirement on the solution of the Dirac equation instead of using the lower order perturbation theory for relatively low intensities on the order of 10^{16} W/cm^2, we compared our theoretical model based on 3D-TDDE with the solution of the time-dependent Schrödinger equation with leading order relativistic corrections (LOPT-TDSE). The procedure we used for the LOPT-TDSE was described in detail in [22]; however, the most essential details are detailed as follows:

Our aim is to obtain the leading order relativistic corrections to the nonrelativistic TDSE describing the evolution of an atomic system. The field-free atomic Hamiltonian including the leading order relativistic corrections (the Breit-Pauli Hamiltonian [24]) differs from the nonrelativistic Hamiltonian in terms of the order of c^{-2}. If we are interested in the corrections of the order of c^{-1} only, we may therefore still use the nonrelativistic expression for the field-free atomic Hamiltonian.

For the nonrelativistic atom-field interaction Hamiltonian, we use the velocity gauge,

$$\hat{H}_{\rm int}^{\rm nr}(t) = \hat{p} \cdot A(t) + \frac{\hat{A}^2(t)}{2}, \tag{9}$$

where $\boldsymbol{A}(t)$ is the vector potential of the pulse, which is the nonrelativistic dipole approximation as a function of the time variable only. Relativistic corrections to this Hamiltonian arise from the fact that the vector potential of a traveling wave is a function of time and space variables. In the geometry we employ, the laser pulse is polarized along the z direction and propagates along the y axis. Vector potential is then a function $\boldsymbol{A}(t - y/c)$ of the combination $t - y/c$. The leading relativistic correction to operator (9) can be obtained by substituting this expression for the vector potential instead of $\boldsymbol{A}(t)$ in Eq. (9), performing an expansion in powers of c^{-1} and keeping the terms linear in c^{-1}. Following this strategy, we obtain a field-atom interaction operator containing relativistic corrections linear in c^{-1}:

$$\hat{H}_{\rm int}^{\rm r}(\boldsymbol{r}, t) = \hat{p}_z A(t) + \frac{\hat{p}_z y E(t)}{c} + \frac{A(t) E(t) y}{c}, \tag{10}$$

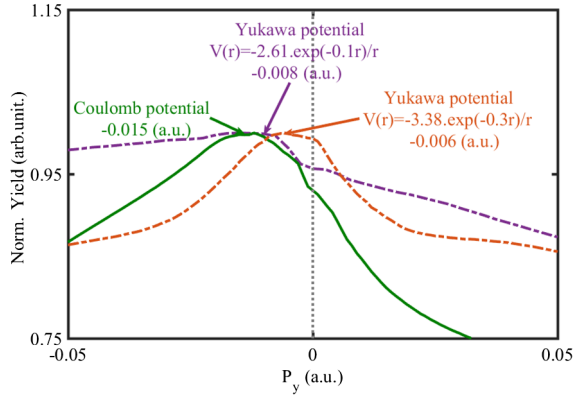

FIG. 5. Coulomb potential has a more pronounced effect on the peak shift with reference to the zero transverse momentum (vertical dotted line). Two different values of Yukawa potential yield a lesser peak shift as compared to the Coulomb potential at the same intensity of 2.5×10^{15} W/cm^2.

where we introduce the electric field of the pulse, $E(t) = -\partial A(t)/\partial t$.

As in the case of the 3D-TDDE, we consider the Ar atom described by means of a SAE model potential [36] as a target system. The LOPT-TDSE with the interaction Hamiltonian was solved using the numerical procedure described in [22].

The results of the simulations based on 3D-TDDE and LOPT-TDSE show the same peak shift and TEMD features at 2.5×10^{15} W/cm^2, as expected. However, at the higher intensity of 1×10^{16} W/cm^2, a substantial qualitative difference in the TEMD features was observed, even if the peak shift remained the same quantitatively (Fig. 6). It is clear from the right panel of Fig. 6 that, at the intensity of 10^{16} W/cm^2, we are entering the regime with the dominating radiation pressure positive peak shift of U_p/c. The model based on 3D-TDDE offers to probe the fine details in the TEMD and provides information about electron dynamics at high intensities.

Furthermore, the effect of CEP on the peak shift was investigated experimentally as well as theoretically. It was found that the CEP dependent peak shift was not resolvable within experimental uncertainty.

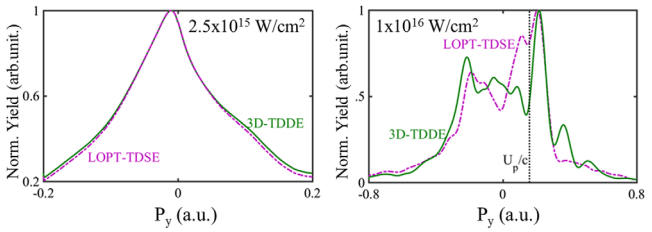

FIG. 6. TEMDs obtained from simulations based on 3D-TDDE and LOPT-TDSE at 1×10^{16} W/cm^2 show quite different features qualitatively as compared to results obtained at lower intensities of 2.5×10^{15} W/cm^2.

In summary, we have presented a comparative theoretical and experimental study of the relativistic nondipole effects emerging at moderately intense laser fields, illustrating the failure of dipole approximation and strong-field approximation, even at laser field intensities commonly considered to be nonrelativistic. The measured and calculated peak shifts in the direction opposite to the laser beam propagation increase with laser intensity due to the Coulomb attraction from the parent ion. Simulations performed for a model Ar atom with Yukawa potential further support this claim. The truly relativistic *ab initio* model based on 3D-TDDE agrees quantitatively with the experimental results. The comparison of our model based on 3D-TDDE with LOPT-TDSE indicates that, although the perturbative approach is sufficiently accurate at lower intensities ($<2.5 \times 10^{15}$ W/cm^2), there are notable differences in the EMD simulated using 3D-TDDE and LOPT-TDSE at 1×10^{16} W/cm^2. With 3D-TDDE being the most advanced theory for the description and analysis of relativistic strong-field effects while being only moderately more computationally demanding, its application for a broad range of intensities is fully justified.

This research was supported by the Australian Research Council Discovery Project No. DP110101894. We also acknowledge support from the Institute for Basic Science, Gwangju, Republic of Korea, under IBS-R012-D1. N. H., A. A., U. S. S. and D. C. are supported by Griffith University International Postgraduate Research Scholarship (GUIPRS). H. X. is supported by an ARC Discovery Early Career Researcher Grant No. DE130101628.

*nida.haram@griffithuni.edu.au
†igorivanov@ibs.re.kr
‡h.xu@griffith.edu.au
§i.litvinyuk@griffith.edu.au
‖r.sang@griffith.edu.au
¶Present address: Solid State Institute, Technion, Haifa 320003, Israel.

[1] H. R. Reiss, Opt. Express **2**, 261 (1998).
[2] C. T. L. Smeenk, L. Arissian, B. Zhou, A. Mysyrowicz, D. M. Villeneuve, A. Staudte, and P. B. Corkum, Phys. Rev. Lett. **106**, 193002 (2011).
[3] A. Ludwig, J. Maurer, B. W. Mayer, C. R. Phillips, L. Gallmann, and U. Keller, Phys. Rev. Lett. **113**, 243001 (2014).
[4] A. Rudenko, K. Zrost, T. Ergler, A. B. Voitkiv, B. Najjari, V. L. B. de Jesus, B. Feuerstein, C. D. Schrter, R. Moshammer, and J. Ullrich, J. Phys. B **38**, L191 (2005).
[5] I. Ivanov, A. Kheifets, J. Calvert, S. Goodall, X. Wang, H. Xu, A. Palmer, D. Kielpinski, I. Litvinyuk, and R. Sang, Sci. Rep. **6**, 19002 (2016).
[6] Y. Huismans *et al.*, Science **331**, 61 (2011).
[7] X.-B. Bian and A. D. Bandrauk, Phys. Rev. Lett. **108**, 263003 (2012).

[8] M. W. Walser, C. H. Keitel, A. Scrinzi, and T. Brabec, Phys. Rev. Lett. **85**, 5082 (2000).
[9] T. Zuo, A. Bandrauk, and P. Corkum, Chem. Phys. Lett. **259**, 313 (1996).
[10] M. Meckel, D. Comtois, D. Zeidler, A. Staudte, D. Pavičić, H. C. Bandulet, H. Pépin, J. C. Kieffer, R. Dörner, D. M. Villeneuve, and P. B. Corkum, Science **320**, 1478 (2008).
[11] C. I. Blaga, J. Xu, A. D. DiChiara, E. Sistrunk, K. Zhang, P. Agostini, T. A. Miller, L. F. DiMauro, and C. Lin, Nature (London) **483**, 194 (2012).
[12] H. Yun, J. Mun, S. Hwang, S. Park, I. Ivanov, C. Nam, and K. Kim, Nat. Photonics **12**, 620 (2018).
[13] A. S. Titi and G. W. F. Drake, Phys. Rev. A **85**, 041404(R) (2012).
[14] J. Liu, Q. Z. Xia, J. F. Tao, and L. B. Fu, Phys. Rev. A **87**, 041403 (2013).
[15] H. R. Reiss, Phys. Rev. A **87**, 033421 (2013).
[16] E. Yakaboylu, M. Klaiber, H. Bauke, K. Z. Hatsagortsyan, and C. H. Keitel, Phys. Rev. A **88**, 063421 (2013).
[17] I. A. Ivanov, Phys. Rev. A **91**, 043410 (2015).
[18] S. Chelkowski, A. D. Bandrauk, and P. B. Corkum, Phys. Rev. A **92**, 051401(R) (2015).
[19] J. F. Tao, Q. Z. Xia, J. Cai, L. B. Fu, and J. Liu, Phys. Rev. A **95**, 011402(R) (2017).
[20] P.-L. He, D. Lao, and F. He, Phys. Rev. Lett. **118**, 163203 (2017).
[21] T. Keil and D. Bauer, J. Phys. B **50**, 194002 (2017).
[22] I. A. Ivanov, J. Dubau, and K. T. Kim, Phys. Rev. A **94**, 033405 (2016).
[23] T. Kjellsson, S. Selstø, and E. Lindroth, Phys. Rev. A **95**, 043403 (2017).
[24] I. I. Sobelman, *Introduction to the Theory of Atomic Spectra* (Pergamon, New York, 1972).
[25] C. Smeenk, J. Z. Salvail, L. Arissian, P. B. Corkum, C. T. Hebeisen, and A. Staudte, Opt. Express **19**, 9336 (2011).
[26] A. S. Alnaser, X. M. Tong, T. Osipov, S. Voss, C. M. Maharjan, B. Shan, Z. Chang, and C. L. Cocke, Phys. Rev. A **70**, 023413 (2004).
[27] J. Ullrich, R. Moshammer, A. Dorn, R. Drner, L. P. H. Schmidt, and H. Schmidt-Bcking, Rep. Prog. Phys. **66**, 1463 (2003).
[28] T. Brabec, M. Y. Ivanov, and P. B. Corkum, Phys. Rev. A **54**, R2551 (1996).
[29] P. B. Corkum, Phys. Rev. Lett. **71**, 1994 (1993).
[30] C. Blaga, F. Catoire, P. Colosimo, G. Paulus, H. Muller, P. Agostini, and L. DiMauro, Nat. Phys. **5**, 335 (2009).
[31] W. Quan, Z. Lin, M. Wu, H. Kang, H. Liu, X. Liu, J. Chen, J. Liu, X. T. He, S. G. Chen, H. Xiong, L. Guo, H. Xu, Y. Fu, Y. Cheng, and Z. Z. Xu, Phys. Rev. Lett. **103**, 093001 (2009).
[32] P. A. Korneev, S. V. Popruzhenko, S. P. Goreslavski, T.-M. Yan, D. Bauer, W. Becker, M. Kübel, M. F. Kling, C. Rödel, M. Wünsche, and G. G. Paulus, Phys. Rev. Lett. **108**, 223601 (2012).
[33] H. Liu, Y. Liu, L. Fu, G. Xin, D. Ye, J. Liu, X. T. He, Y. Yang, X. Liu, Y. Deng, C. Wu, and Q. Gong, Phys. Rev. Lett. **109**, 093001 (2012).
[34] D. Comtois, D. Zeidler, H. Ppin, J. C. Kieffer, D. M. Villeneuve, and P. B. Corkum, J. Phys. B **38**, 1923 (2005).
[35] I. A. Ivanov, Phys. Rev. A **90**, 013418 (2014).
[36] A. Sarsa, F. Glvez, and E. Buenda, At. Data Nucl. Data Tables **88**, 163 (2004).